

Two Functions from a Single Photoresist: Tuning Microstructure Degradability from Light-Stabilized Dynamic Materials

Steven C. Gauci, Katharina Ehrmann,* Marvin Gernhardt, Bryan Tuten, Eva Blasco, Hendrik Frisch, Vishakya Jayalatharachchi, James P. Blinco, Hannes A. Houck,* and Christopher Barner-Kowollik*

A photoresist—based on a light-stabilized dynamic material driven by an out-of-equilibrium photo-Diels–Alder reaction of triazolinediones with naphthalenes—whose ability to intrinsically degrade postprinting can be tuned by a simple adjustment of laser intensity during 3D laser lithography is introduced. The resist's ability to form stable networks under green light irradiation that degrade in the dark is transformed into a tunable degradable 3D printing material platform. In-depth characterization of the printed microstructures via atomic force microscopy before and during degradation reveals the high dependency of the final structures' properties on the writing parameters. Upon identifying the ideal writing parameters and their effect on the network structure, it is possible to selectively toggle between stable and fully degradable structures. This simplifies the direct laser writing manufacturing process of multifunctional materials significantly, which typically requires the use of separate resists and consecutive writing efforts to achieve degradable and nondegradable material sections.

analog of the 2D pixel—thus generating complex 3D architectures with sub-100 nm scale resolution.^[2,3] Consequently, these highly resolved structures have been used for applications ranging from cell biology,^[4] microfluidics^[5] to photonics.^[6]

Despite the progress in the realm of 3D printing, most fabricated structures are unalterable since they are irreversibly cross-linked with the concomitant loss of the resin's photoreactivity and typically consist of only one material.^[7–9] However, to push the frontiers in DLW, there is an increasingly critical need to incorporate multiple properties into printed structures, preferentially achieved in a single printing process. Thus, multimaterial printing with programmed adaptability has emerged as an attractive avenue to generate advanced

1. Introduction

Direct laser writing (DLW), also known as 3D laser lithography, is a well-established additive manufacturing technique that allows for the fabrication of near-arbitrary shaped micro- and nanometer-sized objects.^[1] DLW exploits a two-photon polymerization process whereby a pulsed femtosecond laser beam is tightly focused into a photoresist, generating a very small voxel—the 3D

materials with locally tuned chemical compositions and responsiveness.^[10] Gray-tone lithography has become popular for this purpose.^[11,12] While standard photoresists ideally exhibit binary (“black or white”) behavior, i.e., they cure or they do not cure at the chosen printing conditions, gray-tone lithography exploits the nonideal behavior of specific resists, which print in varying qualities (“gray tones”) depending on the printing conditions. Various resist properties can be changed with the printing


S. C. Gauci, K. Ehrmann, M. Gernhardt, B. Tuten, H. Frisch, V. Jayalatharachchi, J. P. Blinco, C. Barner-Kowollik
School of Chemistry and Physics
Queensland University of Technology (QUT)
2 George Street, Brisbane, QLD 4000, Australia
E-mail: katharina.ehrmann@tuwien.ac.at;
christopher.barnerkowollik@qut.edu.au

S. C. Gauci, K. Ehrmann, M. Gernhardt, B. Tuten, H. Frisch, V. Jayalatharachchi, J. P. Blinco, C. Barner-Kowollik
Centre for Materials Science
Queensland University of Technology (QUT)
2 George Street, Brisbane, QLD 4000, Australia

E. Blasco
Institute for Molecular Systems Engineering and Advanced Materials
Heidelberg University
69120 Heidelberg, Germany

H. A. Houck
Department of Chemistry and Institute of Advanced Study
University of Warwick
Library Road, Coventry CV4 7AL, UK
E-mail: hannes.houck@warwick.ac.uk

C. Barner-Kowollik
Institute of Nanotechnology (INT)
Karlsruhe Institute of Technology (KIT)
Hermann-von-Helmholtz-Platz 1
76344 Eggenstein-Leopoldshafen, Germany

 The ORCID identification number(s) for the author(s) of this article can be found under <https://doi.org/10.1002/adma.202300151>.

© 2023 The Authors. Advanced Materials published by Wiley-VCH GmbH. This is an open access article under the terms of the Creative Commons Attribution-NonCommercial License, which permits use, distribution and reproduction in any medium, provided the original work is properly cited and is not used for commercial purposes.

DOI: 10.1002/adma.202300151

conditions, most commonly laser intensity. For example, height (voxel size) and cross-linking density are changed to influence object dimensions, mechanical, and optical properties among others.^[13–18]

Multimaterial structures are inspired by natural systems, where hierarchical architectures significantly influence their mechanical properties. The ability to transfer these properties to DLW can, for example, lead to adaptive and self-healing microstructures.^[19,20] A major step toward fabricating adaptive materials is the ability to erase 3D structures with precision control when desired.^[21,22] Post-DLW erasing is a highly enabling feature used for the removal of redundant support materials to print more complex microstructures such as overhangs, the degradation of cellular scaffolds to foster tissue regeneration, and the cleavage of valves to control the direction of flow. Such erasable parts are typically removed mechanically post-development, or by conventional etching methods, which are usually not selective.^[23] A more elegant approach is to design cleavable photoresists with degradable linkages, which can be triggered selectively by noninvasive stimuli such as light,^[24,25] or even those that are self-destructive^[26,27] thus actively bypassing an erasing mechanism.

Our group has recently reported the development of a photoresist for DLW that is capable of fabricating microstructures that are self-erasable by exposure to “darkness”.^[27] Specifically, we exploited light-stabilized dynamic materials^[28] (LSDM) for a two-step fabrication process to embed light-stabilized and darkness-triggered erasable segments into permanently crosslinked 3D structures obtained from a conventional resist. Herein, we critically advance resist technology by postulating that by altering the writing parameters (e.g., laser intensity) during fabrication, the degradation properties of the direct-laser-written LSDM-based microstructures can be carefully tuned and effectively switched off completely (Figure 1a). We thus report the first instance where a microstructure consisting of both erasable and nonerasable parts can be printed from a single photoresist (Figure 1b). The unprecedented ability to toggle between permanent and fully erasable features significantly simplifies the fabrication of adaptive and multiproperty materials, which would otherwise require separate photoresists.

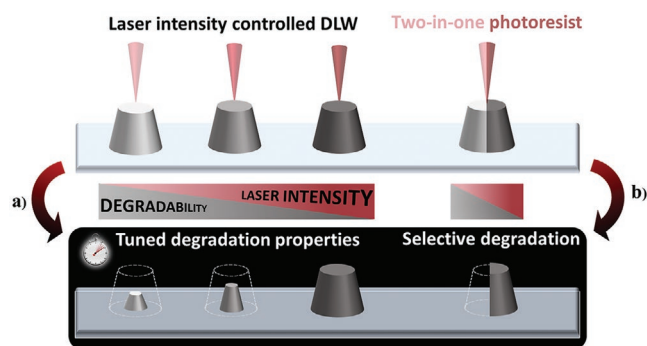


Figure 1. Overview of the present study. a) By altering the laser intensity during the printing process, the degradation properties of the resulting microstructures can be carefully tuned and effectively switched off completely to b) introduce the unprecedented ability to print microstructures via DLW consisting of both degradable and nondegradable segments from a single photoresist.

2. Results and Discussion

2.1. Printing parameter window

We previously established that the LSDM photoresist consisting of a naphthalene-containing polymer (P) and 1,6-hexamethylene bistriazolinedione (BisTAD) (refer to Section S3 in the Supporting Information) can be used to prepare erasable microstars by DLW with delayed degradation when continuously exposed to a green light-emitting diode (LED).^[27] Rather than external regulation of the de-crosslinking, this inspired us to implement time-differentiated structural degradation already during the printing process by altering the writing parameters. Thus, we initiated our study by printing our LSDM-based photoresist at various laser powers to investigate the dependence of degradation on the writing parameters (refer to Section S4 in the Supporting Information). To this end, an array of cone-shaped microstructures was printed in triplicates with a scan speed of $10 \mu\text{m s}^{-1}$ and at laser powers varying between 6.5 and 8.6 mW. This range covers the maximal variability of writing conditions, which produced sufficiently crosslinked networks for stable structures at low power (6.5 mW) yet did not cause microexplosions due to heat evolution in the resist at high power (8.6 mW).^[29] The model used to fabricate arrays of cone-shaped microstructures has a base and top diameter of 10 and $6 \mu\text{m}$, respectively, and a height of $2 \mu\text{m}$ (Figure S14a,b, Supporting Information).

To investigate the effect of laser power on the dimensions of the cone-shaped microstructures post-printing, atomic force microscopy (AFM) was utilized to analyze cone height, diameter of the base, and the diameter at full-width at half maximum (FWHM) (Figure 2). The cone-shaped model was selected to expedite the tracing of each cone with the AFM cantilever (Figure 2a). As depicted in Figure 2, the dimensions of the printed microstructures vary with respect to laser intensity. In all cases, as the laser intensity increases from 6.5 to 8.6 mW, the dimensions of the structures increase, since higher laser intensities increase the curable voxel region during printing.^[30] Specifically, the height of each structure increases from 1.2 to $1.5 \mu\text{m}$ (Figure 2b), while the diameter of the cone base and at FWHM increases from 9.4 to 10.1 and 6.8 to $7.5 \mu\text{m}$, respectively (Figure 2c). With this critical information, the dimensions of the intended structures can be carefully adjusted before printing to enable a seamless integration of degradable and nondegradable segments, which are printed with different laser intensities.

2.2. Degradation behavior

Subsequently, the cone-shaped structures were submerged in tetrahydrofuran (THF) and veiled into darkness at ambient temperature for up to 19 days. THF was utilized to induce swelling and facilitate mobility, which promoted degradation of the material on suitable time scales for our study. The degradation progress was monitored by optical microscopy and by tracing the cone at each degradation stage with an AFM cantilever (Figure 3a, top and bottom, and Figure S15 (Supporting Information)). While all structures show significant

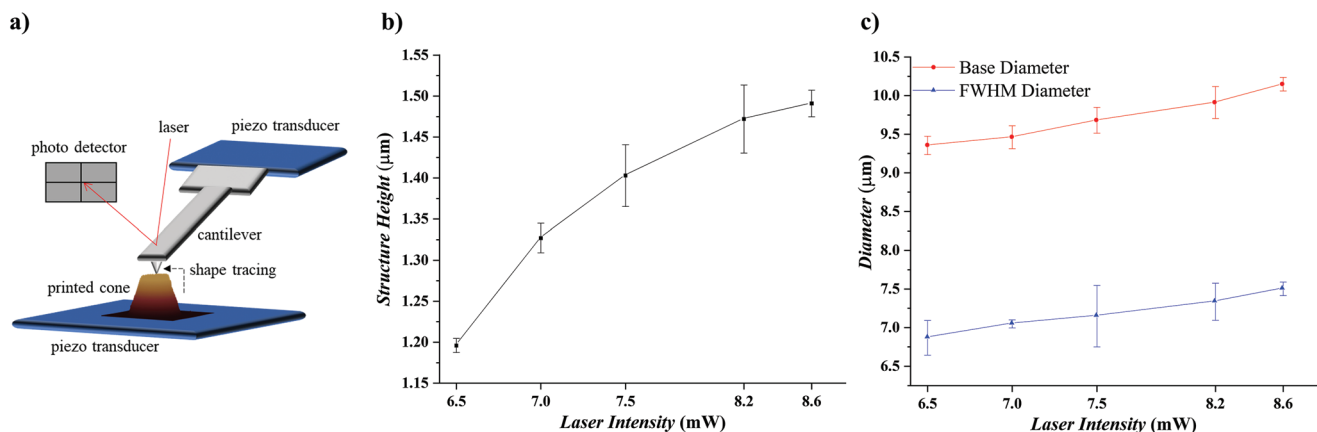


Figure 2. Effect of laser intensity on the dimensions of the microstructures postprinting. a) Illustration of the AFM cantilever tracing the dimensions of a printed cone-shaped microstructure, b) the maximum height of the cone-shaped microstructures, and c) base and FWHM diameter of the resulting microstructures. Each data point represents the average of three specimens and the error bars indicate the standard deviation of the data.

degradation over time, the time scale for this progress varies strongly with the laser intensity employed for writing. For structures written at 6.5 mW, degradation was complete within five days while equally long exposure to darkness of structures written at higher laser powers only resulted in 5–20% degradation due to their higher crosslinking density, increasing structural stability.^[14] Within the observed time frame of 19 days, degradation for laser intensities of 8.6–7 mW plateaus after 12 days and ranges from a 45–80% reduction in cone height.

Interestingly, the degradation progress is nonlinear but reproducibly exhibits rather pronounced degradation plateaus, suggesting a diffusion-controlled degradation mechanism from the outside toward the inner parts of the structure and therefore surface-induced degradation behavior. While the underlying degradation mechanism via a cycloreversion process might suggest bulk degradation behavior, observed surface erosion indicates solvent-induced swelling and thus mobility at the surface of the structures to be an important requirement. Thus

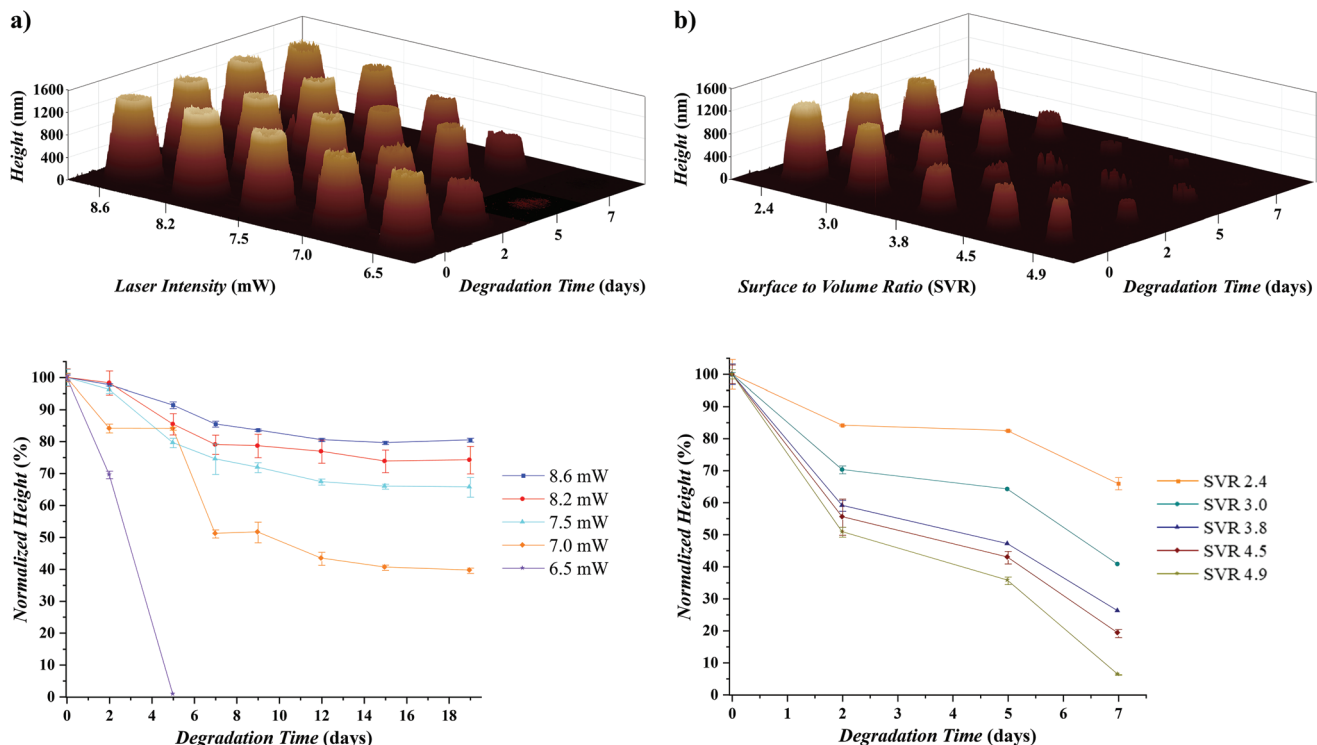


Figure 3. Monitoring of degradation behavior of cone-shaped microstructures immersed in THF in darkness at ambient temperature. a) AFM height data for microstructures fabricated using variable laser intensities as a function of time. b) AFM height data for microstructures with varying SVRs fabricated using 7 mW at several degradation steps. Each data point represents the average of three specimens and the error bars indicate the standard deviation of the data.

the de-crosslinking reaction at the surface occurs faster compared to the bulk. In fact, the microstructures remain largely stable in darkness and in the absence of solvent after 90 days (Figure S16, Supporting Information).

To further investigate the observed plateauing effect during degradation, cone-shaped structures of varying surface-to-volume ratios (SVRs) were printed with a medium laser intensity of 7 mW. While true bulk degradation behavior should be largely uninfluenced by this variation, the rate of surface degradation would increase with increasing surface area compared to the volume of the structure. Thus, the SVR of the structures was tuned from their original value of 2.4 up to a ratio of 4.9, which corresponds to an increase of SVR from 25% to 104%, respectively. These values were calculated from the measured dimensions of each cone with varying SVRs after AFM analysis (Figure S17 and Table S2, Supporting Information). Degradation in THF and darkness at ambient temperature over seven days indeed varied largely for these SVR-altered specimens (Figure 3b, top and bottom, also refer to Figure S18 in the Supporting Information). Furthermore, the plateaus that had been observed previously are also evident in this study and become less pronounced with increasing surface area. It seems that initial swelling of all structures is sufficiently efficient to cause instant degradation on the surface with structures of lower SVR exhibiting lower degradation. The plateau between two and five days, characterizing the delay of degradation until swelling is sufficient, is constant at the two lowest SVRs, while retarded degradation is visible for higher SVRs during this period. Once swelling of the freshly exposed layer is sufficient, degradation is equally fast for all structures printed at the same laser intensity regardless of SVR, which is indicated by the similar relative decrease of all structures between days five and seven. Such an observation is consistent with the assumption that a bulk erosion mechanism indeed occurs, which however, is partly overruled by the effect that swelling of the structures has on the extent of the de-crosslinking. Thus, a phenomenological layer-by-layer degradation of the DLW structures can be observed, which has significant implications on the use of the degradable resist in *in situ* degradation applications. While bulk erosion would continuously deteriorate the mechanical properties of the resist during the degradation process due to chain scissions throughout the network, surface eroding structures mainly decrease in size but maintain their structural integrity until late stages of the degradation process.^[31] Therefore, the supporting nature of the degradable resist can be exploited until late stages of the degradation process, which can be highly desirable in applications where controlled mechanical stability is key.

The role of swelling for degradation speed and mechanism was also confirmed by degradation studies conducted in other solvents than THF, *i.e.*, toluene and dimethylformamide (DMF). For this, cone arrays were printed in triplicates with laser intensities of 8.6, 7.0, and 6.5 mW. Subsequently, the printed structures were immersed in solvent and the degradation progress was monitored via AFM over seven days. In contrast to THF, degradation in toluene occurs significantly slower for cones of all laser intensities (Figure S19, Supporting Information). Meanwhile, cones submerged in DMF do not show signs of degradation over seven days (Figure S20, Supporting Information). Instead, slight differences in swelling

behavior of cones printed at different laser powers indicate a difference in cross-linking density for these specimens. Specifically, the cones printed with the lowest laser intensity (6.5 and 7.0 mW) swell more in comparison to those printed with the highest intensity (8.6 mW) over seven days. Such an observation is also consistent with the fact that only cones printed at the lowest laser intensities exhibit an onset of degradation at day seven, while the cones printed at the highest laser power remain stable. Therefore, this solvent study suggests that degradation of the DLW structures is both dependent on swelling and crosslinking density.

To further investigate if crosslinking density is the primary factor that dictates the observed difference in de-crosslinking kinetics, the chemical nature of the crosslinks arising from different laser intensities was probed in more detail. Since the dynamic covalent behavior of LSDMs is greatly influenced by regioisomer formation,^[28] we hypothesized that changing the laser intensity could alter the ratio of both regioisomer products and thereby affect the overall de-crosslinking kinetics of the resulting materials (Figure S13, Supporting Information). To test this hypothesis, small molecule experiments were performed with monofunctional model compounds. Specifically, a solution of 4-*n*-butyl-triazolinedione and methyl 2-naphthoate in deuterated acetone was subjected to $\lambda = 380$ nm laser irradiation (*i.e.*, $\lambda = \frac{1}{2} \times 780$ nm) with different laser intensities, *e.g.*, 50, 150, and 350 μ J (refer to Sections S2.9 and S3.4 in the Supporting Information). Following 30 min irradiation, the regioisomer ratios were determined via ¹H-NMR analysis (Figure S13, Supporting Information). However, no differentiation in the individual regioisomer fractions could be observed, with 4_A:4_B (40:60) remaining constant with respect to the laser intensity. Thus, the observed difference in material stability seems unlikely to be caused by changes in the chemical regioisomer composition of the cross-links. Nonetheless, the model experiments indicated a significant increase in conversion with increasing laser intensity (*e.g.*, 5–32% going from 50 to 350 μ J), which also suggests an increase in crosslinking density when structures are printed at higher laser powers. Critically, the resulting ¹H-NMR spectra did not indicate any occurrence of secondary modes of reactivity, such as naphthalene photodimers. In addition, control DLW experiments of blank solutions containing either P or BisTAD did not lead to curing of the photoresist.

While this single-photon absorption investigation mimics the two-photon absorption as closely as possible by halving the irradiation wavelength, these irradiation conditions may not reflect the two-photon printing process entirely. Since it is intrinsic to two-photon printing that only extremely small irradiation volumes are cured, it is difficult to conduct bulk studies with this curing mechanism. Furthermore, solution-based irradiations only approximate the curing environment in a photoresist. Therefore, we further investigated the chemical composition of the actual structures fabricated via the two-photon absorption process. Specifically, single-layered squares (15 × 15 × 1 μ m³) were direct-laser-written from the LSDM-based resist at the highest (8.6 mW) and lowest (6.5 mW) laser intensities and analyzed by time-of-flight secondary ion mass spectrometry (TOF-SIMS) (refer to Section S4.3 and Figure S24 in the Supporting Information). A careful principal component

analysis of the observed fragments obtained from the highest laser intensity written structures did not indicate chemically different compositions compared to the structures fabricated at the lowest laser intensity (Table S3 and Figures S25–S27, Supporting Information). These results unambiguously confirm that the laser intensity only affects the crosslinking density and does not lead to chemically different materials.

2.3. Multimaterial printing

Having thoroughly investigated the degradation properties of the printed microstructures, the LSDM-based photoresist was employed to embed both erasable and nonerasable segments within the same 3D multimaterial structure. Thus far, imparting degradable properties to a single 3D structure has only been achieved by sequentially assembling the structure using separate photoresists. When fabricating complex 3D architectures, however, this strategy becomes extremely challenging for two main reasons. First, it is often difficult and thus time-consuming to locate the printed structure following the photoresist exchange. Second, building suspended geometries in between an existing framework—or directly over a support block—requires precision accuracy, which increases the com-

plexity of the writing process significantly. By using our LSDM-based photoresist, however, we circumvent these challenges by simply switching the laser intensity from 8.6 to 6.5 mW during the fabrication process, thereby enabling the fabrication of multifunctional 3D structures from a single photoresist where segments can be selectively removed (Figure 4a). Three experiments were conducted to demonstrate this unprecedented two-in-one printing functionality by comparing the printed structures before and after degradation via scanning electron microscopy (SEM) imaging. In the first example, we encoded a message within the original structure, which became visible upon degradation in THF at ambient temperature for five days (889 → 007, Figure 4b). Critically, the height of the degradable parts was increased to 120% compared to the height of the nondegradable part (100%, as per Figure 2b) to allow for a seamless transition between the degradable and nondegradable segments. It is important to note that without this adjustment, there is a significant difference in height between both segments (Figure S21, Supporting Information). In addition, optical microscopic imaging was employed to visualize the degradation process of the encoded message after three days in THF (Figure S22, Supporting Information). In the second example, we showed partial degradability of a 3D structure to demonstrate the LSDM-based resist's

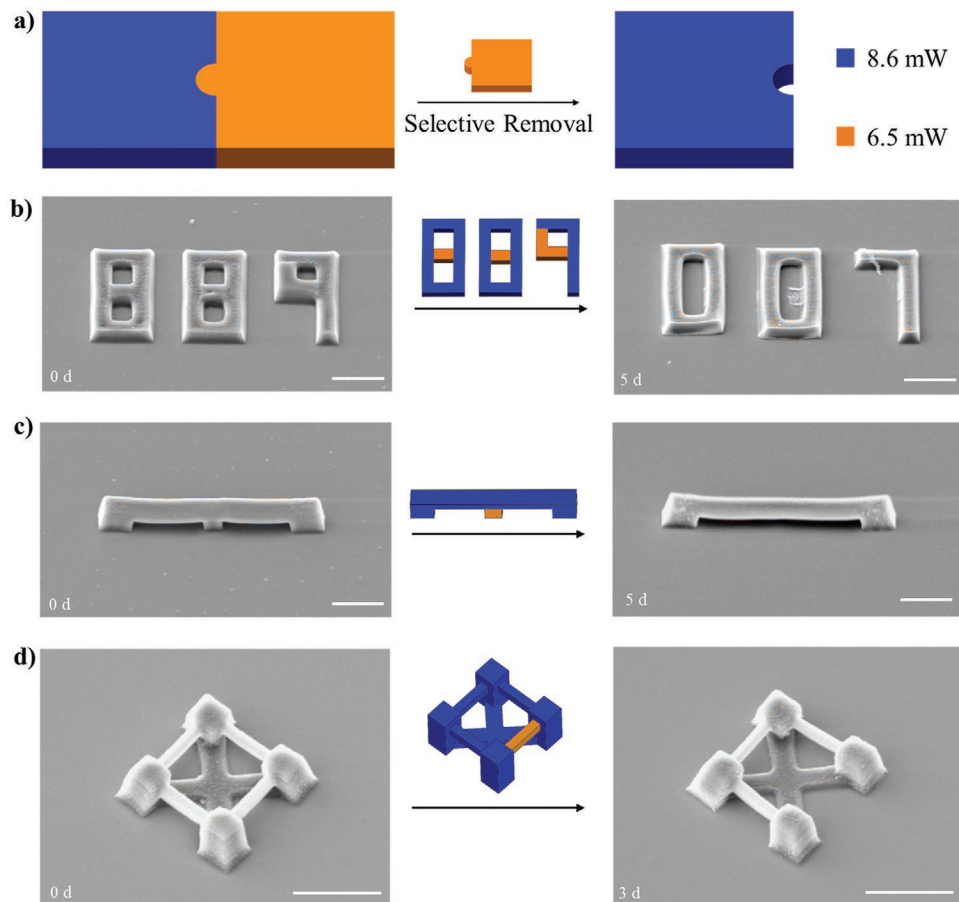


Figure 4. 3D DLW demonstration with the LSDM-based photoresist. a) Visual representation of a multifunctional structure fabricated from a single photoresist, where switching the laser intensity from 8.6 to 6.5 mW during fabrication allows segments to be selectively removed post-printing. b–d) SEM images post-printing (left), and after being immersed in THF in the dark at ambient temperature (right) (scale bars, 10 μm).

utility in advanced structures where supporting structures are necessary to print the geometry. Initially, a series of bridges were fabricated from the LSDM-based resist to investigate the maximum distance where features could be printed unsupportedly (Figure S23, Supporting Information). Whereas distances up to 20 μm were fabricated without requiring support, strong bending was visible during the printing process when the distance was increased to 30 μm , resulting in the bridge to fracture and separate into two parts. Thus, a support block was incorporated into the bridge model to prevent bending and to facilitate the connection between both sides of the bridge (Figure 4c). Again, the height of the degradable segment was increased by 120% to compensate for height differences arising from different laser writing intensities, hence allowing for the underside of the bridge to print directly onto the support block. Subsequently, the structure was immersed in THF for five days to remove the support block and obtain the unsupported bridge, which could not be fabricated without the LSDM-based support. For the final example, we fabricated a scaffold-type structure where a specific segment within the 3D architecture was selectively erased (Figure 4d). We chose this design to highlight our resist's ability to fabricate full-3D architectures, which could serve as a template to monitor how cells respond to a changing 3D environment.^[22,32] In contrast to the earlier examples, degradation of the specific bridge within the scaffold was achieved after only three days in THF. Since this erasable segment is suspended between the two pillars, only slight degradation is required before the bridge can detach and diffuse away from the remaining scaffold before being completely de-crosslinked.

3. Conclusion

In summary, we have introduced the first example where 3D structures consisting of both degradable and nondegradable segments can be printed via DLW from a single photoresist. Specifically, we utilized AFM to thoroughly investigate the high dependency of laser intensity during the printing process on the degradation properties of the LSDM-based structures. We demonstrate that by altering the laser intensity during the printing process, we are able to fabricate multifunctional 3D microstructures exclusively from our LSDM-based resist, which significantly simplifies the manufacturing process. In combination with the surface erosion-like behavior, printing at two different laser intensities demonstrates the ability to use one photoresist for spatially resolved degradation of a structure, which largely maintains its structural integrity throughout its full lifetime. Detailed degradation studies with varying surface–volume ratios and solvents as well as chemical analysis of model molecules and of the printed resist via principal component analysis of TOF-SIMS data led to the conclusion that increasing crosslinking density at higher laser intensity is responsible for the highly tunable degradation behavior. The ability to toggle between degradable and nondegradable segments from a single photoresist constitutes a critical advancement in DLW, where complex 3D architectures can be printed using a simple one-step fabrication strategy.

Supporting Information

Supporting Information is available from the Wiley Online Library or from the author.

Acknowledgements

C.B.-K. and H.F. acknowledge funding from the Australian Research Council (ARC) in the form of a Laureate Fellowship (C.B.-K. Grant No. FL170100014) enabling the author's photochemical research program and a DECRA Fellowship (H.F.) as well as continued key support from the Queensland University of Technology (QUT). S.C.G. gratefully acknowledges QUT for a Ph.D. Research Scholarship. E.B. and C.B.-K. acknowledge key funding by the Deutsche Forschungsgemeinschaft (DFG, German Research Foundation) under Germany's Excellence Strategy for the Excellence Cluster "3D Matter Made to Order" (Grant No. EXC-2082/1-390761711), by the Carl Zeiss Foundation and the Helmholtz program "Materials Systems Engineering." The Central Analytical Research Facility (CARF) at QUT is gratefully acknowledged for access to analytical instrumentation, supported by QUT's Research Portfolio. H.A.H. acknowledges funding of his EUTOPIA-SIF fellowship received from the European Union's Horizon 2020 research and innovation programme under the Marie Skłodowska-Curie grant agreement No. 945380, and mobility funding received from the Institute of Advanced Study (IAS) at the University of Warwick. This work was performed in part at the Queensland node of the Australian National Fabrication Facility, a company established under the National Collaborative Research Infrastructure Strategy to provide nano- and microfabrication facilities for Australia's researchers.

Open access publishing facilitated by Queensland University of Technology, as part of the Wiley - Queensland University of Technology agreement via the Council of Australian University Librarians.

Conflict of Interest

The authors declare no conflict of interest.

Data Availability Statement

The data that support the findings of this study are available from the corresponding author upon reasonable request.

Keywords

direct laser writing, erasable microstructures, gray-tone lithography, light-stabilized dynamic materials

Received: January 5, 2023

Revised: February 17, 2023

Published online: March 29, 2023

- [1] M. Carlotti, O. Tricinci, V. Mattoli, *Adv. Mater. Technol.* **2022**, 7, 2101590.
- [2] J. Fischer, M. Wegener, *Laser Photonics Rev.* **2013**, 7, 22.
- [3] K.-S. Lee, R. H. Kim, D.-Y. Yang, S. H. Park, *Prog. Polym. Sci.* **2008**, 33, 631.
- [4] B. Richter, V. Hahn, S. Bertels, T. K. Claus, M. Wegener, G. Delaitte, C. Barner-Kowollik, M. Bastmeyer, *Adv. Mater.* **2017**, 29, 1604342.

- [5] B.-B. Xu, Y.-L. Zhang, H. Xia, W.-F. Dong, H. Ding, H.-B. Sun, *Lab Chip* **2013**, *13*, 1677.
- [6] K. K. Seet, V. Mizeikis, S. Matsuo, S. Juodkakis, H. Misawa, *Adv. Mater.* **2005**, *17*, 541.
- [7] C. A. Spiegel, M. Hippler, A. Münchinger, M. Bastmeyer, C. Barner-Kowollik, M. Wegener, E. Blasco, *Adv. Funct. Mater.* **2020**, *30*, 1907615.
- [8] F. Momeni, S. M. Mehdi Hassani N, X. Liu, J. Ni, *Mater. Des.* **2017**, *122*, 42.
- [9] C. M. González-Henríquez, M. A. Sarabia-Vallejos, J. Rodríguez-Hernandez, *Prog. Polym. Sci.* **2019**, *94*, 57.
- [10] Z. Xiong, M.-L. Zheng, X.-Z. Dong, W.-Q. Chen, F. Jin, Z.-S. Zhao, X.-M. Duan, *Soft Matter* **2011**, *7*, 10353.
- [11] M. Hippler, E. Blasco, J. Qu, M. Tanaka, C. Barner-Kowollik, M. Wegener, M. Bastmeyer, *Nat. Commun.* **2019**, *10*, 232.
- [12] B. Kaehr, J. B. Shear, *Proc. Natl. Acad. Sci. USA* **2008**, *105*, 8850.
- [13] X. Kuang, J. Wu, K. Chen, Z. Zhao, Z. Ding, F. Hu, D. Fang, H. J. Qi, *Sci. Adv.* **2019**, *5*, eaav5790.
- [14] J. Qu, M. Kadic, A. Naber, M. Wegener, *Sci. Rep.* **2017**, *7*, 40643.
- [15] Y. Liu, R. Liu, J. Qiu, S. Wang, *Adv. Manuf.* **2022**, *4*, e10107.
- [16] F. Ugarak, G. Ulliac, J. A. I. Martinez, J. Moughames, V. Laude, M. Kadic, A. Mosset, *Materials* **2022**, *15*, 4070.
- [17] T. Aderneuer, O. Fernández, R. Ferrini, *Opt. Express* **2021**, *29*, 39511.
- [18] F. Gao, J. Yao, Y. Zeng, S. Xie, Y. Guo, Z. Cui, *Microelectron. Eng.* **2002**, *61*, 165.
- [19] A. R. Studart, *Chem. Soc. Rev.* **2016**, *45*, 359.
- [20] N. D. Dolinski, Z. A. Page, E. B. Callaway, F. Eisenreich, R. V. Garcia, R. Chavez, D. P. Bothman, S. Hecht, F. W. Zok, C. J. Hawker, *Adv. Mater.* **2018**, *30*, 1800364.
- [21] H. A. Houck, P. Müller, M. Wegener, C. Barner-Kowollik, F. E. Du Prez, E. Blasco, *Adv. Mater.* **2020**, *32*, 2003060.
- [22] C. Barner-Kowollik, M. Bastmeyer, E. Blasco, G. Delaittre, P. Müller, B. Richter, M. Wegener, *Angew. Chem., Int. Ed.* **2017**, *56*, 15828.
- [23] D. Gräfe, S. L. Walden, J. Blinco, M. Wegener, E. Blasco, C. Barner-Kowollik, *Angew. Chem., Int. Ed.* **2020**, *59*, 6330.
- [24] R. Batchelor, T. Messer, M. Hippler, M. Wegener, C. Barner-Kowollik, E. Blasco, *Adv. Mater.* **2019**, *31*, 1904085.
- [25] M. Gernhardt, V. X. Truong, C. Barner-Kowollik, *Adv. Mater.* **2022**, *34*, 2203474.
- [26] Y. Gao, K. Sim, X. Yan, J. Jiang, J. Xie, C. Yu, *Sci. Rep.* **2017**, *7*, 947.
- [27] S. C. Gauci, M. Gernhardt, H. Frisch, H. A. Houck, J. P. Blinco, E. Blasco, B. T. Tuten, C. Barner-Kowollik, *Adv. Funct. Mater.* **2022**, 2206303.
- [28] H. A. Houck, E. Blasco, F. E. Du Prez, C. Barner-Kowollik, *J. Am. Chem. Soc.* **2019**, *141*, 12329.
- [29] J. B. Mueller, J. Fischer, Y. J. Mange, T. Nann, M. Wegener, *Appl. Phys. Lett.* **2013**, *103*, 123107.
- [30] C.-S. Shin, T.-J. Li, C.-L. Lin, *Micromachines* **2018**, *9*, 615.
- [31] H. Zhang, L. Zhou, W. Zhang, *Tissue Eng., Part B* **2014**, *20*, 492.
- [32] A. M. Greiner, F. Klein, T. Gudzenko, B. Richter, T. Striebel, B. G. Wundari, T. J. Autenrieth, M. Wegener, C. M. Franz, M. Bastmeyer, *Biomaterials* **2015**, *69*, 121.